Optimal Planetary Rendezvous with an Electric Sail

Mingying Huo [a], Giovanni Mengali [b] and Alessandro A. Quarta [b,*]

[a] *Department of Aerospace Engineering, Harbin Institute of Technology, Harbin 150006, China*

[b] *Department of Civil and Industrial Engineering, University of Pisa, I-56122 Pisa, Italy*

Abstract

Electric Solar Wind Sail-based missions towards Venus and Mars are discussed in this paper. The analysis takes into account the real three-dimensional shape of both starting and arrival orbits and the planetary ephemeris constraints, using the JPL planetary ephemerides model DE405/LE405. Each mission is parameterized with different values of departure date and spacecraft characteristic acceleration, the latter representing the maximum propulsive acceleration when the Sun-spacecraft distance is one astronomical unit. The transfer trajectories are studied in an optimal framework, using a Gauss pseudospectral method in which the initial guesses for state and control histories are obtained with a genetic algorithm-based approach. In particular, the paper illustrates the numerical simulations obtained with a spacecraft characteristic acceleration of one millimeter per second squared and the results cover a range of launch dates of seventeen years. Finally, a parametric study of the transfer's flight time corresponding to the optimal departure dates is also discussed, for different values of the spacecraft characteristic acceleration.

Key words: Electric solar wind sail, Venus and Mars missions, Optimal rendezvous

* Corresponding author.
Email addresses: huomingying123@gmail.com (Mingying Huo), g.mengali@ing.unipi.it (Giovanni Mengali), a.quarta@ing.unipi.it (Alessandro A. Quarta).

Nomenclature

$\boldsymbol{a}$	=	propulsive acceleration, with $a \triangleq \|\boldsymbol{a}\|$ [$\mathrm{mm/s^2}$]
a_c	=	spacecraft characteristic acceleration [$\mathrm{mm/s^2}$]
C	=	spacecraft center-of-mass
$\hat{\boldsymbol{i}}$, $\hat{\boldsymbol{j}}$, $\hat{\boldsymbol{k}}$	=	reference frame's unit vectors
J	=	performance index [days]
$\boldsymbol{r}$	=	spacecraft position vector, with $r \triangleq \|\boldsymbol{r}\|$ [au]
S	=	Sun's center-of-mass
t	=	time [days]
$\mathbb{T}$	=	transformation matrix between $\mathcal{T}_O$ and $\mathcal{T}_\odot$
$\mathcal{T}$	=	reference frame
$\boldsymbol{u}$	=	control vector
$\boldsymbol{v}$	=	spacecraft velocity vector [km/s]
$\boldsymbol{x}$	=	state vector
α	=	cone angle [deg]
δ	=	clock angle [deg]
ϕ	=	spacecraft's azimuthal angle [deg]
$\mu_\odot$	=	Sun's gravitational parameter [$\mathrm{km^3/s^2}$]
τ	=	switching parameter
θ	=	spacecraft's polar angle [deg]

Subscripts

0	=	initial, parking orbit

f	=	final, target orbit
max	=	maximum
O	=	orbital
$\oplus$	=	Earth
$\odot$	=	Sun, inertial
$\triangle$	=	target planet

Superscripts

$\cdot$	=	time derivative

1 Introduction

The recent success of the Japanese pioneering mission IKAROS (Interplanetary Kite-craft Accelerated by Radiation Of the Sun), where a photonic solar sail was first deployed in the interplanetary space (Tsuda et al., 2011a,b), has demonstrated the potential feasibility of using propellantless propulsion systems for robotic missions to the deep space. As a matter of fact, even though the spacecraft maximum propulsive acceleration was still too low for practical purposes, nevertheless IKAROS is definitely a successful mission, in that it showed the actual possibility of changing a spacecraft interplanetary orbit by photonic thrust. Such a milestone result opens new and interesting mission opportunities that would be very difficult to perform with conventional propulsion systems, due to the severe constraints related to the propellant consumption.

Among the few propellantless propulsion systems that have been studied so far for the robotic

exploration of the Solar System, the Electric Solar Wind Sail (E-sail), proposed by Pekka Janhunen about ten years ago (Janhunen, 2004), is one of the most promising options. An E-sail based spacecraft is constituted by a central structure (main body) to which a number of long tethers are attached. The tethers are stretched by spinning the spacecraft around an axis and are maintained at a high positive potential by means of a solar-powered electron gun, see Fig. 1.

[Figure 1 about here.]

The solar wind ions are repelled by the positive E-sail tethers in such a way that some momentum is extracted from the solar wind flow and a net thrust is produced. The tethers spin-plane can also be oriented, within some limits, by regulating the potential of each tether (Janhunen et al., 2010). As a result, the thrust direction may be inclined of an angle $\alpha > 0$, referred to as cone angle, with respect to the Sun-spacecraft (radial) direction. Simulation analyses by Janhunen (2010) show that the maximum value of the cone angle cannot exceed $\alpha_{\max} \triangleq \max(\alpha) \approx 35\,\text{deg}$. The possibility of thrust orientation allows the vehicle's angular momentum to be varied and, as such, an E-sail based spacecraft may perform a classical interplanetary rendezvous mission between non-coplanar orbits. It is worth noting that the capability of producing a non-negligible circumferential thrust component makes the E-sail performance better than other conceptually similar solutions, such as the classical magnetic sail (Zubrin and Andrews, 1991; Love and Andrews, 1992; Funaki et al., 2007), or the more recent mini-magnetospheric plasma thruster (Winglee et al., 2000, 2003).

In the last few years a number of scientific papers have appeared to analyze the E-sail performance in different potential missions, including the study of interplanetary transfers, the generation of artificial equilibrium points (Aliasi et al., 2013), the achievement of non-Keplerian orbits (Mengali and Quarta, 2009), or the study of an escape from the Solar System (Mengali et al., 2008a; Quarta and Mengali, 2010). In particular, a first estimate of the E-sail perfor-

mance for an interplanetary transfer was discussed by Mengali et al. (2008b). In that paper the acceleration thrust was assumed to vary with the Sun-spacecraft distance r proportional to $(1/r)^{7/6}$. However, subsequent plasma dynamic simulations (Janhunen, 2010, 2009) have shown that the E-sail thrust per tether length is five times higher than what previously estimated, i.e. about 500 nN/m at $r = r_{\oplus} \triangleq 1$ au (roughly corresponding to 1 N thrust for a total tether length of 2000 km) and, more important from a mission analysis viewpoint, the thrust modulus scales proportional to $1/r$.

The aim of this paper is to reappraise the performance of an E-sail based spacecraft in a classical interplanetary transfer to an inner (Venus) and an outer planet (Mars), using a thrust modulus that varies as $1/r$ with the distance from the Sun. In particular, for each of the two mission scenarios, the optimal analysis allows the minimum transfer time to be found (using a direct approach) as a function of the E-sail performance using a realistic set of planetary ephemeris data within a time-range of seventeen years. The E-sail performance is usually quantified in terms of spacecraft characteristic acceleration a_c, which corresponds to the maximum propulsive acceleration at a distance from the Sun equal to 1 au. The value of a_c in general depends on the payload mass and on the technological characteristics of the E-sail, such as the tethers' number and their length. For example, using the parametric mass budget model described by Janhunen et al. (2013), a spacecraft with a payload mass of 100 kg, propelled by an E-sail with 44 tethers (of 15.4 km each), is able to produce a characteristic acceleration of about 1 mm/s^2. In this paper the problem is therefore parameterized as a function of the value of the spacecraft characteristic acceleration, and the simulation results for a mission scenario in which $a_c = 1$ mm/s^2 are presented.

2 Mathematical Model

The equations of motion for an E-sail based spacecraft in a heliocentric-ecliptic inertial reference frame $\mathcal{T}_\odot\,(S; x,\, y,\, z)$ are

$$\dot{\boldsymbol{r}} = \boldsymbol{v} \tag{1}$$

$$\dot{\boldsymbol{v}} = -\frac{\mu_\odot}{r^3}\,\boldsymbol{r} + \tau\,\boldsymbol{a} \tag{2}$$

where $\mu_\odot$ is the Sun's gravitational parameter, $\boldsymbol{r}$ is the spacecraft position vector (see Fig. 2), $\boldsymbol{v}$ is the spacecraft velocity vector, $\boldsymbol{a}$ is the E-sail propulsive acceleration vector and $\tau \in [0,\, 1]$ is the switching parameter that models the thruster on/off condition and is introduced to account for the existence of coasting arcs in the spacecraft trajectory.

[Figure 2 about here.]

Bearing in mind the constraint on the maximum value of cone angle (i.e. the value of $\alpha_{\max}$), the propulsive acceleration vector $\boldsymbol{a}$ is more conveniently written in an orbital reference frame $\mathcal{T}_O\,(C; x_O,\, y_O,\, z_O)$, whose origin is at the spacecraft center-of-mass C. The z_O-axis of the orbital frame is along the Sun-spacecraft direction, which coincides with the approximate direction of propagation of the solar wind, see Fig. 2. The three unit vectors of the orbital reference frame are defined as

$$\hat{\boldsymbol{k}}_O \triangleq \boldsymbol{r}/r \qquad , \qquad \hat{\boldsymbol{j}}_O \triangleq \frac{\hat{\boldsymbol{k}} \times \hat{\boldsymbol{k}}_O}{\|\hat{\boldsymbol{k}} \times \hat{\boldsymbol{k}}_O\|} \qquad , \qquad \hat{\boldsymbol{i}}_O \triangleq \hat{\boldsymbol{j}}_O \times \hat{\boldsymbol{k}}_O \tag{3}$$

where $\hat{\boldsymbol{k}}$ is the unit vector of the (inertial) z-axis. To avoid singularities, in the special case $\hat{\boldsymbol{k}} \times \hat{\boldsymbol{k}}_O = 0$, i.e. when the spacecraft belongs to the z-axis of the inertial reference frame $\mathcal{T}_\odot$, the second equation in (3) is substituted by $\hat{\boldsymbol{j}}_O \equiv \hat{\boldsymbol{j}}$, where $\hat{\boldsymbol{j}}$ is the unit vector of the y-axis.

When the propulsion system is switched on (that is when $\tau \neq 0$), the propulsive acceleration vector $\boldsymbol{a}$ can be conveniently expressed in the orbital reference frame as a function of both the cone angle $\alpha \in [0,\, \alpha_{\max}]$ and the clock angle $\delta \in [-\pi,\, \pi]$ as

$$[\boldsymbol{a}]_{\mathcal{T}_O} = a_c \left(\frac{r_\oplus}{r}\right) [\sin\alpha\, \cos\delta,\ \sin\alpha\, \sin\delta,\ \cos\alpha]^{\mathrm{T}} \tag{4}$$

where δ, positive if measured counterclockwise with respect to the z_O-axis, is the angle between the direction of x_O and the projection of $\boldsymbol{a}$ onto the plane (x_O, y_O), see Fig. 2. Note that, according to Janhunen (2010, 2009), the propulsive acceleration modulus $a = \|\boldsymbol{a}\|$ actually varies proportional to the inverse distance from the Sun.

The components of the propulsive acceleration vector $\boldsymbol{a}$ in the inertial reference frame are obtained from the relationship

$$[\boldsymbol{a}]_{\mathcal{T}_\odot} = \mathbb{T}\, [\boldsymbol{a}]_{\mathcal{T}_O} \tag{5}$$

where $\mathbb{T}$ is a suitable transformation matrix, whose entries are functions of the polar angle $\theta \in [0,\, \pi]$ and of the azimuthal angle $\phi \in [0,\, 2\pi]$, see Fig. 2. The transformation matrix is found to be

$$\mathbb{T} = \begin{bmatrix} \cos\phi, & -\sin\phi, & 0 \\ \sin\phi, & \cos\phi, & 0 \\ 0, & 0, & 1 \end{bmatrix} \begin{bmatrix} \cos\theta, & 0, & \sin\theta \\ 0, & 1, & 0 \\ -\sin\theta, & 0, & \cos\theta \end{bmatrix} = \begin{bmatrix} \cos\phi\cos\theta, & -\sin\phi, & \cos\phi\sin\theta \\ \cos\theta\sin\phi, & \cos\phi, & \sin\phi\sin\theta \\ -\sin\theta, & 0, & \cos\theta \end{bmatrix} \tag{6}$$

Note that all of the entries of $\mathbb{T}$ can be equivalently written as a function of the components of the position vector in the inertial frame $[\boldsymbol{r}]_{\mathcal{T}_\odot} \triangleq [r_x,\, r_y,\, r_z]^{\mathrm{T}}$ using the following relationships

$$\sin\theta = \frac{\sqrt{r_x^2 + r_y^2}}{r} \quad , \quad \cos\theta = \frac{r_z}{r} \quad , \quad \sin\phi = \frac{r_y}{\sqrt{r_x^2 + r_y^2}} \quad , \quad \cos\phi = \frac{r_x}{\sqrt{r_x^2 + r_y^2}} \tag{7}$$

where $r = \sqrt{r_x^2 + r_y^2 + r_z^2}$ is the Sun-spacecraft distance.

Taking into account Eqs. (1)–(2) and (4)–(7), the spacecraft equations of motion can be written in compact form as

$$\dot{\boldsymbol{x}}(t) = \boldsymbol{f}\left(\boldsymbol{x},\, \boldsymbol{u},\, t\right) \tag{8}$$

where $\boldsymbol{x} \triangleq [r_x,\, r_y,\, r_z,\, v_x,\, v_y,\, v_z]^{\mathrm{T}}$ is the state vector (being v_x, v_y, and v_z the components of the velocity vector $\boldsymbol{v}$ in the inertial frame, i.e. $[\boldsymbol{v}]_{\mathcal{T}_\odot} = [v_x,\, v_y,\, v_z]^{\mathrm{T}}$), and $\boldsymbol{u} \triangleq [\alpha,\, \delta,\, \tau]^{\mathrm{T}}$ is the control vector. Note that the constraint on the cone angle is given by

$$\alpha \leq \alpha_{\max} \tag{9}$$

which must be considered only when the propulsion system is switched on (i.e. when $\tau \neq 0$).

The differential system describing the spacecraft dynamics is hence constituted by the six scalar nonlinear equations that are obtained by projecting Eq. (8) onto the inertial frame, and is completed by assigning the initial condition vector $\boldsymbol{x}_0$, constituted by the three components of the position vector and the three components of the velocity vector, calculated at the initial time t_0 (corresponding to the launch date). In particular, the vector $\boldsymbol{x}_0$ is constituted by the components of the Earth's position and velocity vectors at time t_0, viz.

$$[\boldsymbol{x}_0]_{\mathcal{T}_\odot} = \left[\boldsymbol{x}_{0_\oplus}\right]_{\mathcal{T}_\odot} \triangleq \left[r_{x_{0\oplus}},\, r_{y_{0\oplus}},\, r_{z_{0\oplus}},\, v_{x_{0\oplus}},\, v_{y_{0\oplus}},\, v_{z_{0\oplus}}\right]^{\mathrm{T}} \tag{10}$$

Note that Eq. (10) is representative of a situation in which the spacecraft heliocentric transfer follows an Earth escape with zero hyperbolic excess velocity with respect to the planet. In the succeeding analysis the orbit propagation of the Earth and the other planets involved in the simulations is performed by means of the JPL planetary ephemerides model DE405/LE405 (Standish, 1998).

2.1 Trajectory Optimization

The optimal control law, that is, the time history of the triplet (α, δ, τ), is found by minimizing the flight time necessary to perform a rendezvous with the target planet (either Venus or Mars in the simulations discussed in this paper) for a given initial time t_0. The problem amounts to minimizing the scalar performance index

$$J \triangleq t_f - t_0 \tag{11}$$

where t_f is the final time. The optimal control law must take into account both the constraint on the cone angle given by Eq. (9), and the final rendezvous condition, viz.

$$[\boldsymbol{x}_f]_{\mathcal{T}_\odot} = \left[\boldsymbol{x}_{f_\triangle}\right]_{\mathcal{T}_\odot} \triangleq \left[r_{x_{f\triangle}},\, r_{y_{f\triangle}},\, r_{z_{f\triangle}},\, v_{x_{f\triangle}},\, v_{y_{f\triangle}},\, v_{z_{f\triangle}}\right]^{\mathrm{T}} \tag{12}$$

where $\boldsymbol{x}_{f_\triangle}$ is the state vector of the target planet at the end of flight, i.e. when $t = t_f$, the latter being an output of the optimization process.

The minimum-time rendezvous problem was solved by using a hybrid genetic algorithm and a pseudospectral method. The latter is an implementation of the Gauss pseudospectral method described by Benson (2005), which transcribes the continuous optimal control problem into a discrete nonlinear programming problem (NLP) by means of global polynomial approximations to the differential equations at a set of Legendre-Gauss points. The transcribed NLP can be solved by sequential quadratic programming, which however needs the designer to provide the initial state and control histories. The Gauss pseudospectral method is generally robust to the initial guess. However, some cases exist in which the initial-guess subproblem is a critical point of the optimization process. To alleviate such a problem, a genetic algorithm is therefore used to conduct a random search within the space of feasible solutions and provide a reasonable initial guess for the state and control histories used in the NLP. As a result, the hybrid optimization

method is able to look for the optimal solution without any external guess from the designer. A detailed description of the whole hybrid algorithm can be found in the recent paper by Qi et al. (2014).

3 Numerical Simulations

The previous optimization problem was solved to find the minimum transfer times for a Earth-Venus and an Earth-Mars heliocentric transfer. The problem was addressed by varying the launch date, in a parametric way, between the 1st January 2014 and the 1st January 2031, thus exploring a launch window of 17 years. The launch date was varied with a step size of 30 days. Assuming a spacecraft characteristic acceleration $a_c = 1\,\mathrm{mm/s^2}$, the simulation results are summarized in Fig. 3(a) for the Earth-Venus transfer, and in Fig. 3(b) for the Earth-Mars mission scenario.

[Figure 3 about here.]

The optimal transfer times as a function of the launch date show a recurring behavior. The time interval between two launch dates providing the same transfer time is close to the synodic period of the two planets (about 780 days for Mars, and 583 days for Venus). This result is by no means surprising, due to the small inclination and the nearly circular shape of the orbits of Mars and Venus. Figure 3 also shows that within the selected time interval of 17 years the minimum transfer time is 323 days for Mars, with an optimal launch date on 20 April 2016, and 205 days for Venus, with an optimal launch date on 14 December 2027.

When the characteristic acceleration is varied in the range $a_c \in [0.5,\, 1.1]\,\mathrm{mm/s^2}$, the optimal transfer times are summarized in Table 1, which, as expected, shows an increase of transfer times when the value of a_c is reduced.

[Table 1 about here.]

The optimal flight times are close to the absolute minima, which can be obtained by looking for the optimal transfers between the starting and the arrival orbits using an ephemeris-free model, i.e. a transfer without any constraint on the initial and final spacecraft's position. The latter problem was solved with an indirect method, and the best points along the starting and arrival orbits were found to minimize the total flight time. Figure 4 also shows a comparison between the absolute minima in an ephemeris-free model (continuous line) and the optimal results in an ephemeris-constrained mission scenario (circles) obtained with the direct approach, see also Table 1. Note that the simulation results in an ephemeris-free model are useful to check the validity of the corresponding results obtained in an ephemeris-constrained scenario.

[Figure 4 about here.]

3.1 Case study

Assuming an optimal Earth-Venus transfer with a spacecraft characteristic acceleration of $1\,\mathrm{mm/s^2}$ and the optimal launch date of Table 1 (14 December 2027), the transfer trajectory is illustrated in Fig. 5. Note that the z-axis scale is intentionally exaggerated to better visualize the three-dimensionality of the trajectory.

[Figure 5 about here.]

Figures 6 and 7 show the three components of the position and velocity vectors (in the inertial frame $\mathcal{T}_\odot$) for the spacecraft and the two planets involved in the simulation. The time histories of the control angles α and δ are illustrated in Fig. 8, where it is worth noting the existence of a coasting arc in the optimal trajectory. This result is in accordance with the optimal control law found with an indirect approach and discussed by Mengali et al. (2008b).

[Figure 6 about here.]

[Figure 7 about here.]

[Figure 8 about here.]

The second case study involves an Earth-Mars transfer with $a_c = 1\,\mathrm{mm/s^2}$ and an optimal launch date corresponding to 21 April 2016, see Table 1. The optimal transfer trajectory is shown in Fig. 9, the components of the position and velocity vectors are illustrated in Figs. 10 and 11, while the time histories of the control angles are reported in Fig. 12.

[Figure 9 about here.]

[Figure 10 about here.]

[Figure 11 about here.]

[Figure 12 about here.]

4 Conclusions

Electric solar wind sail based rendezvous missions towards Venus and Mars have been investigated in this paper. The analysis takes into account both the real three-dimensional shape of the starting and arrival orbits and the ephemeris constraints. Each mission is parameterized with different values of starting time, and the results show that the flight time fluctuates periodically with the starting time. The direct optimization algorithm, which combines a genetic algorithm to provide an initial guess for the state and control histories, with a Gauss pseudospectral method to translate the continuous optimal control problem into a discrete nonlinear programming problem, is able to find solutions in an efficient way. The results, obtained with a launch window range of 17 years, provide optimal solutions close to the absolute minima

that can be found with an indirect approach and an ephemeris-free model. The simulation times for an Earth-Mars and an Earth-Venus rendezvous transfers, obtained with a spacecraft characteristic acceleration of one millimeter per second squared, confirm the competitiveness of such a propellantless propulsion system and motivates a further in-depth analysis of this kind of propulsion technology. In this respect, the results reported in the paper represent a starting point for a more detailed system analysis that includes a mass breakdown model.

5 Acknowledgments

The first author wish to thank the Shanghai Aerospace Science and Technology Foundation of China (Grant no. SAST201312).

References

Aliasi, G., Mengali, G., and Quarta, A. A. (2013). "Artificial equilibrium points for electric sail with constant attitude". *Journal of Spacecraft and Rockets*, Vol. 50, No. 6, pp. 1295–1298. doi:10.2514/1.A32540.

Benson, D. (2005). *A Gauss Pseudospectral Transcription for Optimal Control*. Ph.D. Thesis, Massachusetts Institute of Technology. Retrievable at http://hdl.handle.net/1721.1/28919.

Funaki, I., Kojima, H., Yamakawa, H., Nakayama, Y., and Shimizu, Y. (2007). "Laboratory experiment of plasma flow around magnetic sail". *Astrophysics and Space Science*, Vol. 307, No. 1–3, pp. 63–68. doi:10.1007/s10509-006-9251-4.

Janhunen, P. (2004). "Electric sail for spacecraft propulsion". *Journal of Propulsion and Power*, Vol. 20, No. 4, pp. 763–764. doi:10.2514/1.8580.

Janhunen, P. (2009). "Increased electric sail thrust through removal of trapped shielding

electrons by orbit chaotisation due to spacecraft body". *Annales Geophysicae*, Vol. 27, pp. 3089–3100. doi:10.5194/angeo-27-3089-2009.

Janhunen, P. (2010). "The electric solar wind sail status report". In "European Planetary Science Congress 2010", Vol. 5. Rome, Italy. Paper EPSC 2010-297.

Janhunen, P., Quarta, A. A., and Mengali, G. (2013). "Electric solar wind sail mass budget model". *Geoscientific Instrumentation, Methods and Data Systems*, Vol. 2, No. 1, pp. 85–95. doi:10.5194/gi-2-85-2013.

Janhunen, P. et al. (2010). "Electric solar wind sail: Towards test missions". *Review of Scientific Instruments*, Vol. 81, No. 11, pp. 111301–1–111301–11. doi:10.1063/1.3514548.

Love, S. G. and Andrews, D. G. (1992). "Applications of magnetic sails". *Acta Astronautica*, Vol. 26, No. 8–10, pp. 643–651. doi:10.1016/0094-5765(92)90154-B.

Mengali, G. and Quarta, A. A. (2009). "Non-keplerian orbits for electric sails". *Celestial Mechanics and Dynamical Astronomy*, Vol. 105, No. 1–3, pp. 179–195. doi:10.1007/s10569-009-9200-y.

Mengali, G., Quarta, A. A., and Janhunen, P. (2008a). "Considerations of electric sailcraft trajectory design". *Journal of the British Interplanetary Society*, Vol. 61, pp. 326–329.

Mengali, G., Quarta, A. A., and Janhunen, P. (2008b). "Electric sail performance analysis". *Journal of Spacecraft and Rockets*, Vol. 45, No. 1, pp. 122–129. doi:10.2514/1.31769.

Qi, N., Huo, M., and Yuan, Q. (2014). "Displaced electric sail orbits design and transition trajectory optimization". *Mathematical Problems in Engineering*, Vol. 2014, pp. 1–9. doi:10.1155/2014/932190. Article ID 932190.

Quarta, A. A. and Mengali, G. (2010). "Electric sail mission analysis for outer solar system exploration". *Journal of Guidance, Control, and Dynamics*, Vol. 33, No. 3, pp. 740–755. doi:10.2514/1.47006.

Standish, E. M. (1998). "JPL planetary and lunar ephemerides, DE405/LE405". Interoffice Memoradum IOM 312.F-98-048, Jet Propulsion Laboratory. Available online (cited January 21, 2008) `http://iau-comm4.jpl.nasa.gov/de405iom/de405iom.pdf`.

Tsuda, Y., Mori, O., Funase, R., Hirotaka, S., Yamamoto, T., Saiki, T., Endo, T., Yonekura, K., Hoshino, H., and Kawaguchi, J. (2011a). "Achievement of IKAROS - japanese deep space solar sail demonstration mission". In G. Genta, ed., "Missions to the Outer Solar System and Beyond", Seventh IAA Symposium on Realistic Near-Term Advanced Scientific Space Missions, Aosta, Italy.

Tsuda, Y., Mori, O., Funase, R., Sawada, H., Yamamoto, T., Saiki, T., Endo, T., and Kawaguchi, J. (2011b). "Flight status of IKAROS deep space solar sail demonstrator". *Acta Astronautica*, Vol. 69, No. 9-10, pp. 833–840. doi:10.1016/j.actaastro.2011.06.005.

Winglee, R. M., Euripides, P., Ziemba, T., Slough, J., and Giersch, L. (2003). "Simulation of mini-magnetospheric plasma propulsion (M2P2) interacting with an external plasma wind". In "39th Joint Propulsion Conference and Exhibition", Huntsville. AIAA Paper 2003-5225.

Winglee, R. M., Slough, J., Ziemba, T., and Goodson, A. (2000). "Mini-magnetospheric plasma propulsion: Tapping the energy of the solar wind for spacecraft propulsion". *Journal of Geophysical Research*, Vol. 105, No. A9, pp. 21,067–21,078.

Zubrin, R. M. and Andrews, D. G. (1991). "Magnetic sails and interplanetary travel". *Journal of Spacecraft and Rockets*, Vol. 28, No. 2, pp. 197–203. doi:10.2514/3.26230.

acceleration	Earth-Venus transfer		Earth-Mars transfer	
a_c [mm/s^2]	flight time [days]	launch date	flight time [days]	launch date
1.1	201	13-Dec.-2027	318	21-Apr.-2016
1	205	14-Dec.-2027	323	21-Apr.-2016
0.9	210	13-Dec.-2027	331	17-Apr.-2016
0.8	216	11-Dec.-2027	343	9-Apr.-2016
0.7	225	7-Dec.-2027	357	30-Mar.-2016
0.6	236	1-Dec.-2027	377	6-Feb.-2029
0.5	254	22-Nov.-2027	401	1-Feb.-2029

Table 1
Minimum flight time and optimal starting date as a function of the spacecraft characteristic acceleration for an Earth-Venus and Earth-Mars transfer.

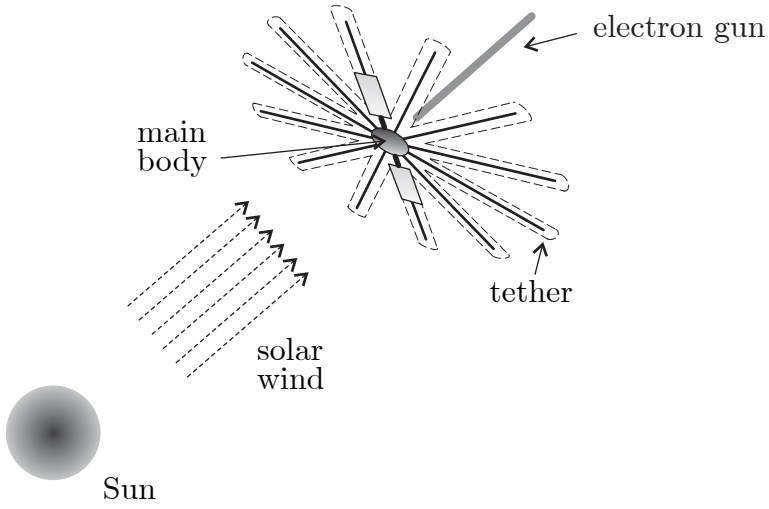

Figure 1. Conceptual scheme of the E-sail propulsion system in the interplanetary space.

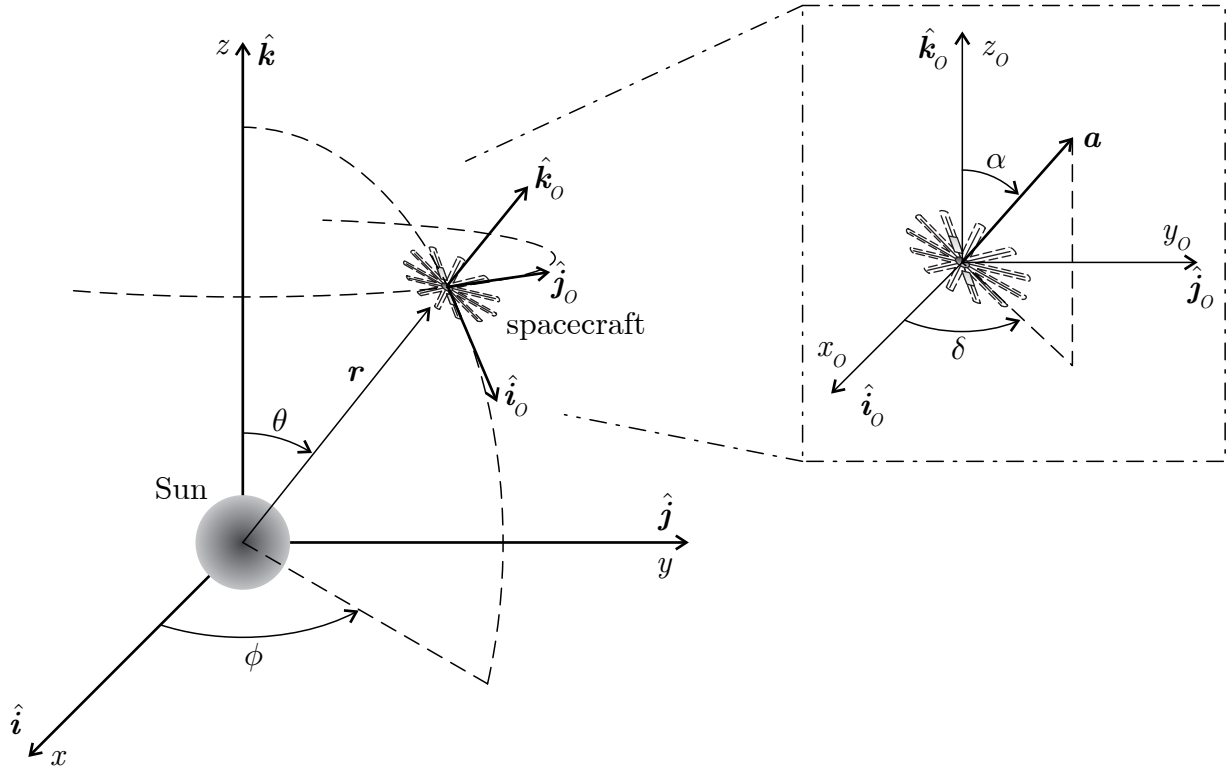

Figure 2. Reference frames and propulsive acceleration's characteristic angles.

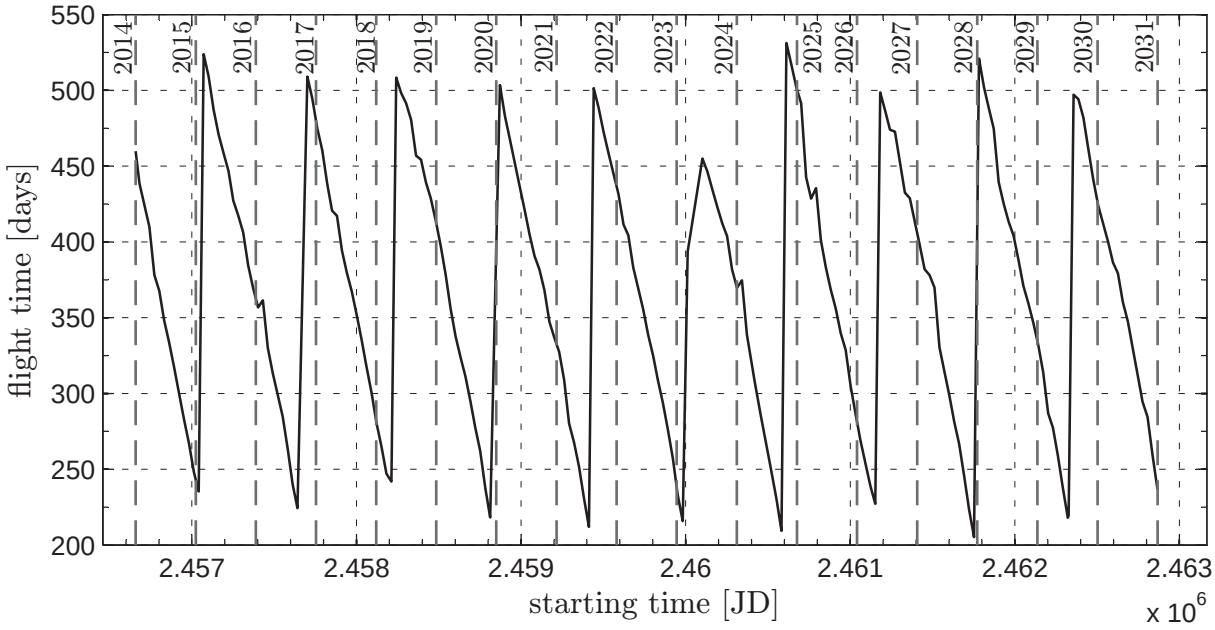

(a) Earth-Venus rendezvous.

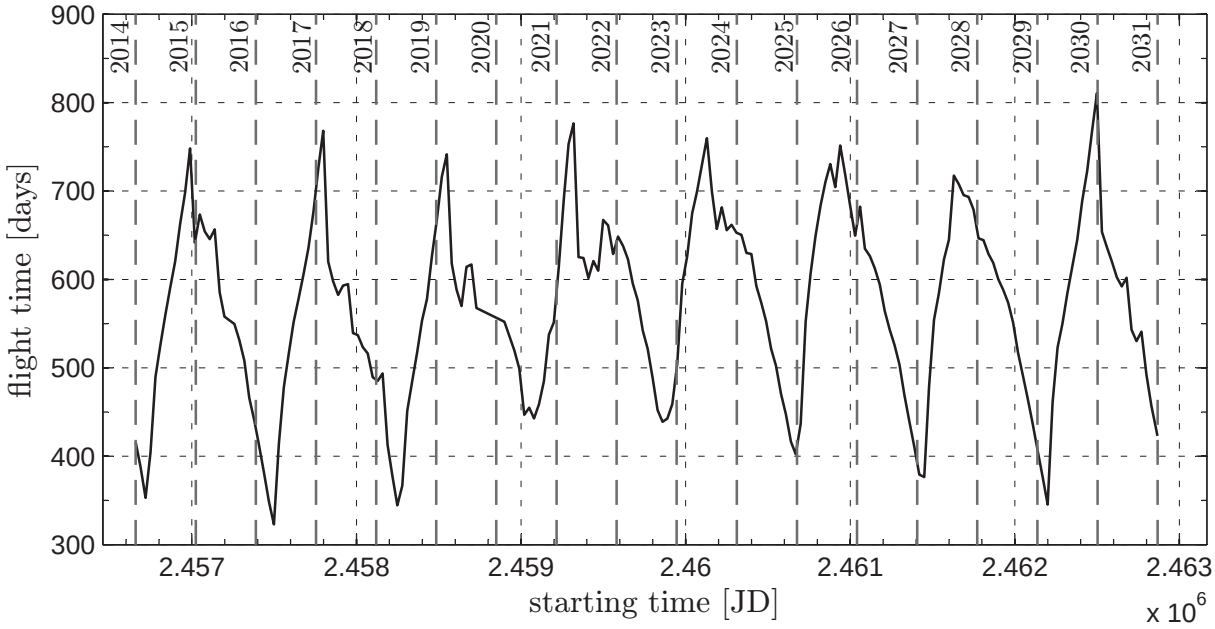

(b) Earth-Mars rendezvous.

Figure 3. Minimum flight times as a function of the starting date (when $a_c = 1$ mm/s^2) for an Earth-Venus and Earth-Mars transfer.

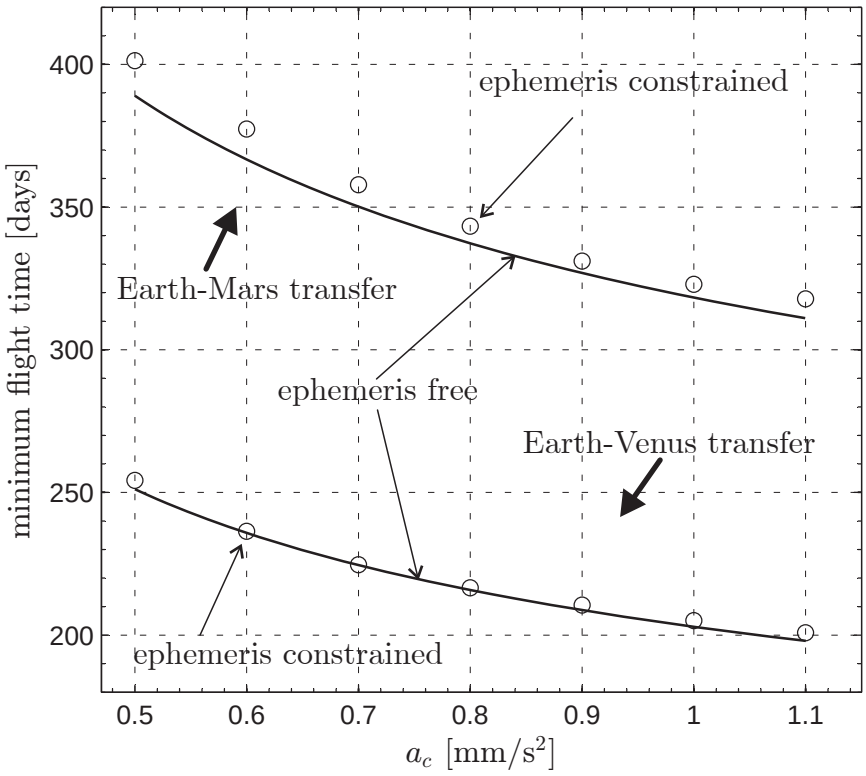

Figure 4. Minimum flight times for an ephemeris-free and an ephemeris-constrained mission scenario.

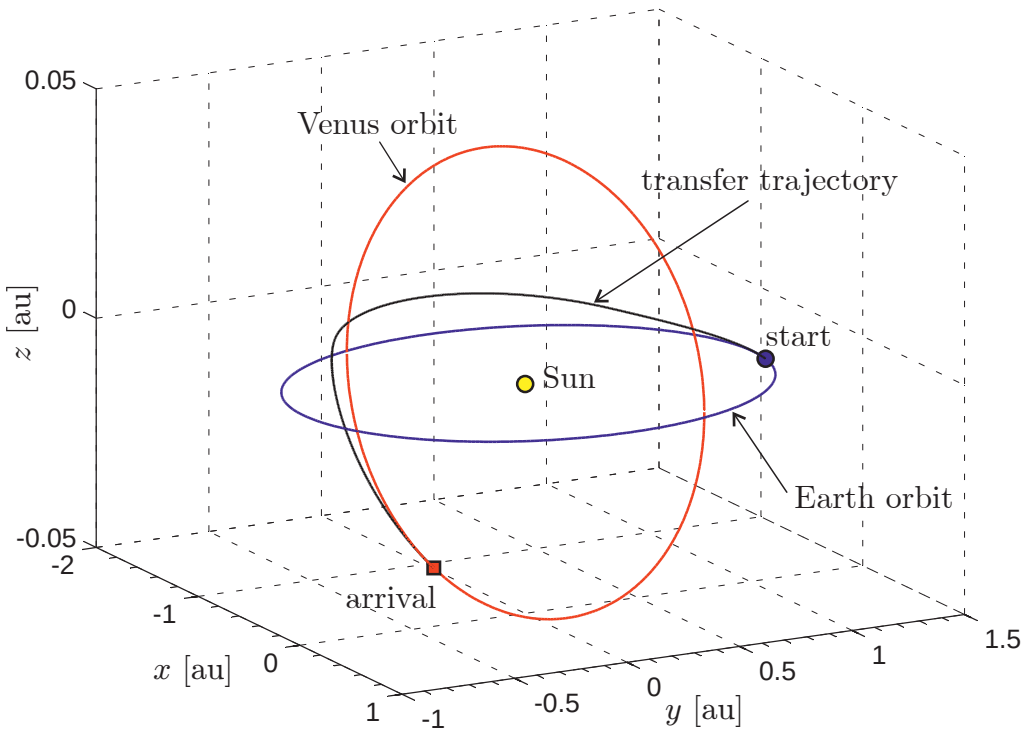

Figure 5. Earth-Venus optimal transfer orbit with a start on 14 December 2027 using a characteristic acceleration of 1 mm/s^2.

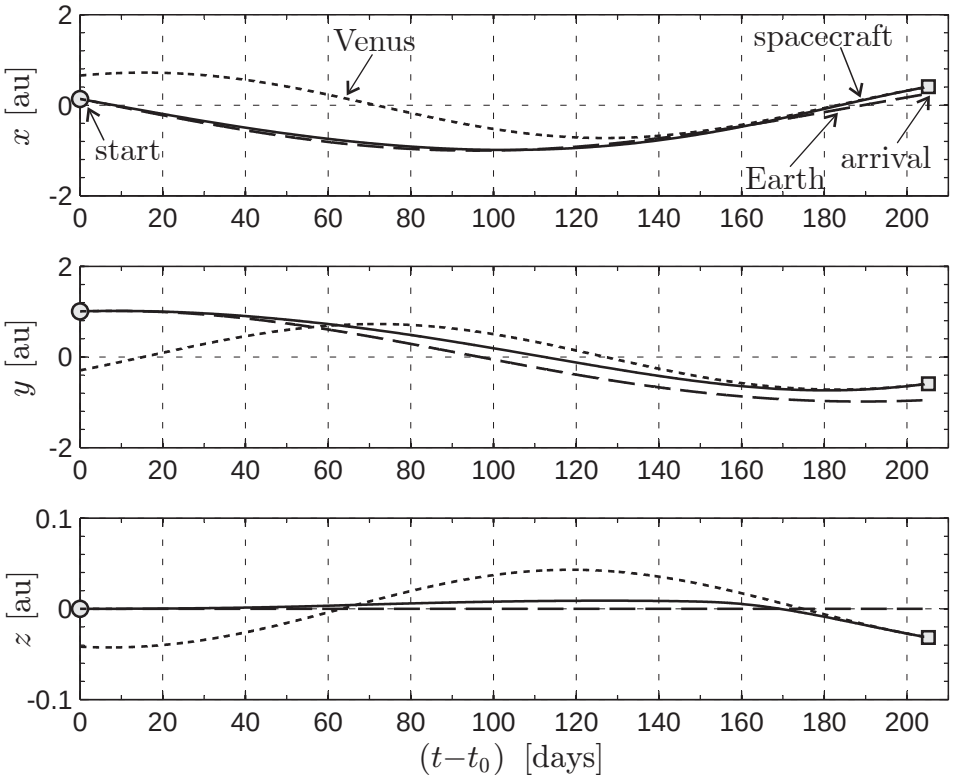

Figure 6. Components (in the inertial frame) of the position vector as a function of time, for an Earth-Venus optimal transfer with $a_c = 1$ mm/s^2 and a starting date on 14 December 2027.

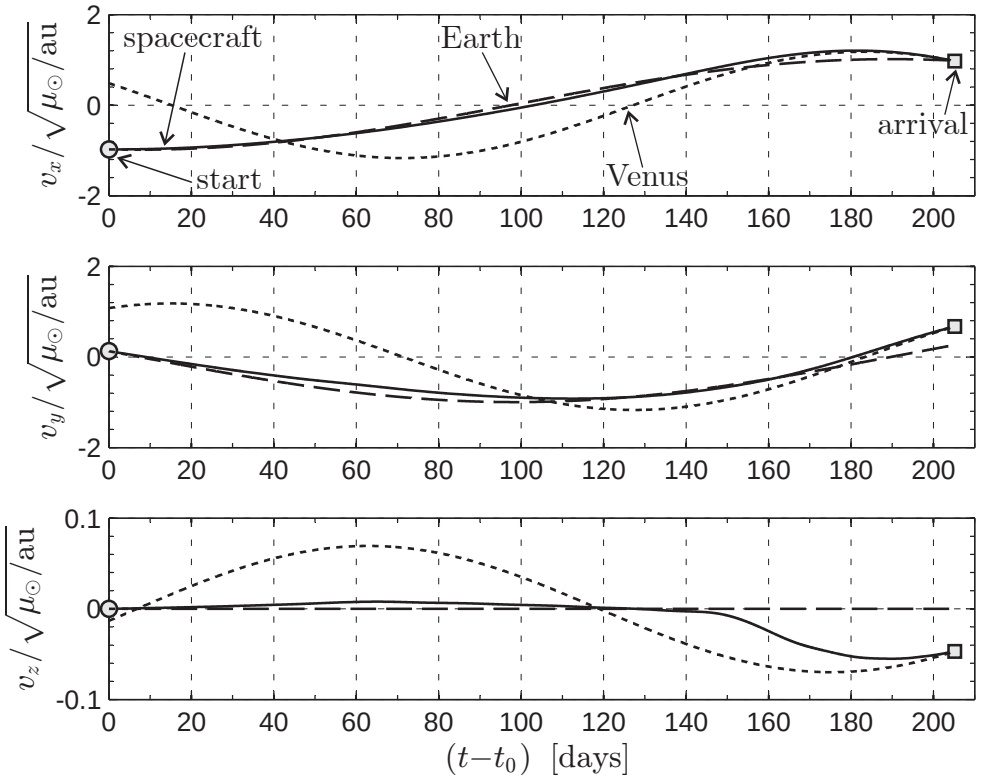

Figure 7. Dimensionless components (in the inertial frame) of the velocity vector as a function of time, for an Earth-Venus optimal transfer with $a_c = 1$ mm/s^2 and a starting date on 14 December 2027.

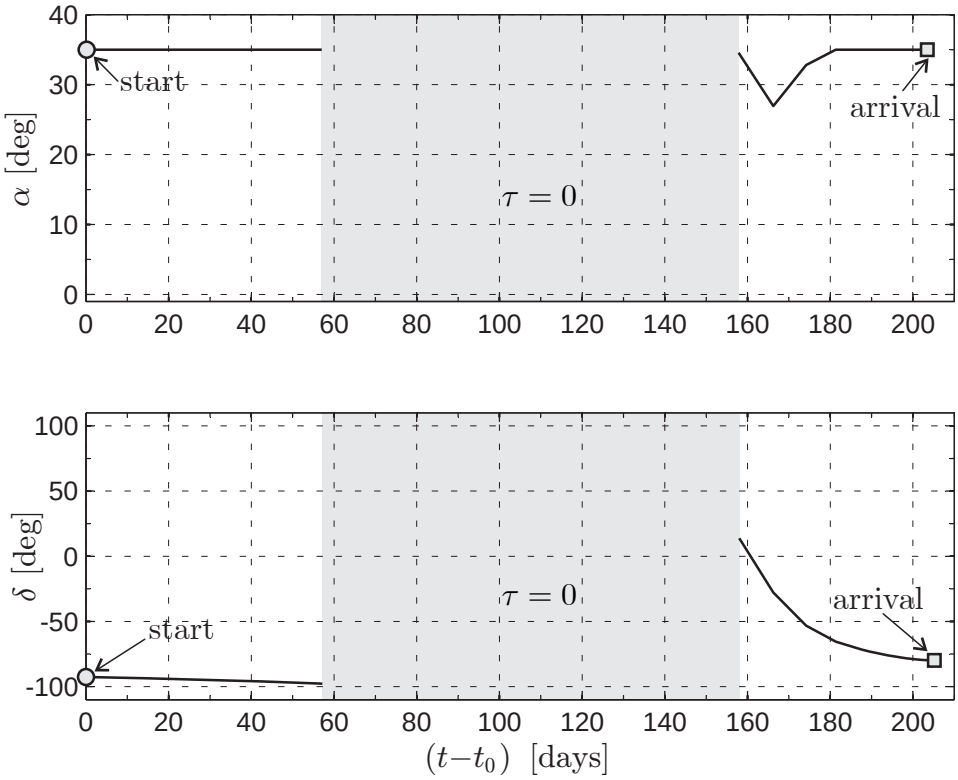

Figure 8. Thrust angles and switching parameter as a function of time, for an Earth-Venus optimal transfer with $a_c = 1$ mm/s^2 and a starting date on 14 December 2027.

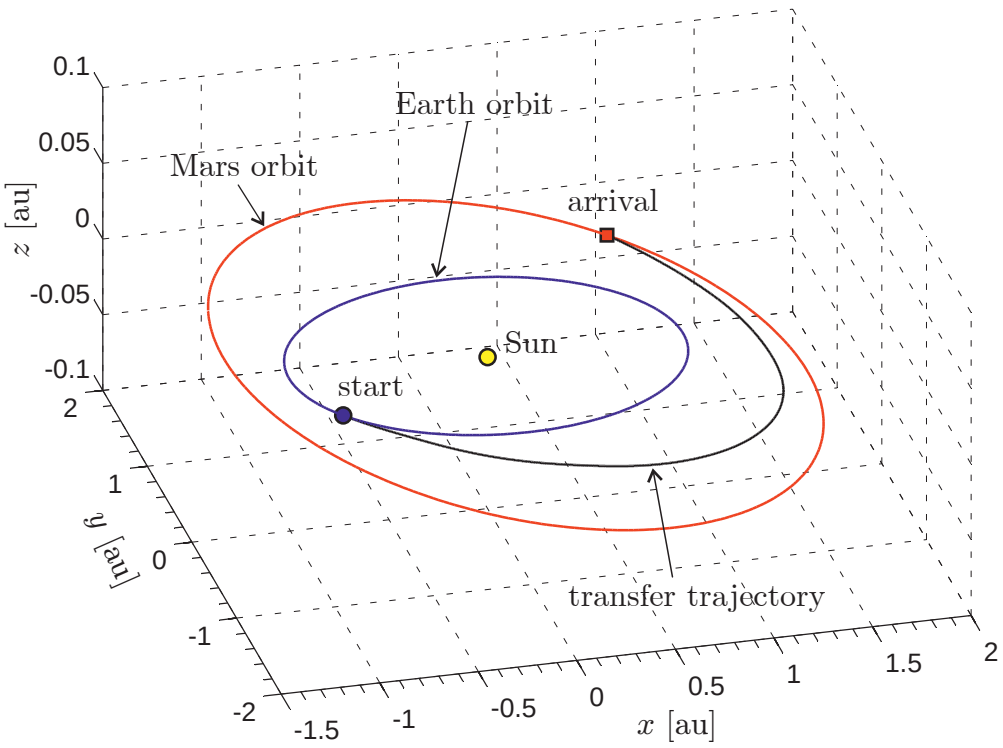

Figure 9. Earth-Mars optimal transfer trajectory with $a_c = 1$ mm/s^2 and a starting date on 21 April 2016.

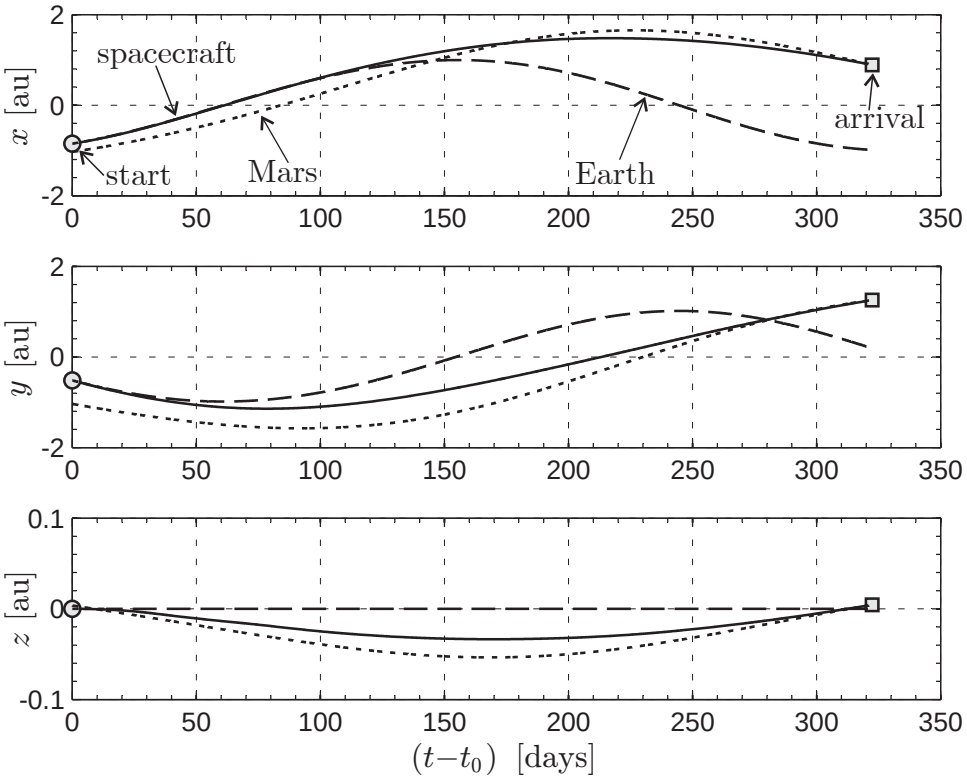

Figure 10. Components (in the inertial frame) of the position vector as a function of time, for an Earth-Mars optimal transfer with $a_c = 1$ mm/s^2 and a starting date on 21 April 2016.

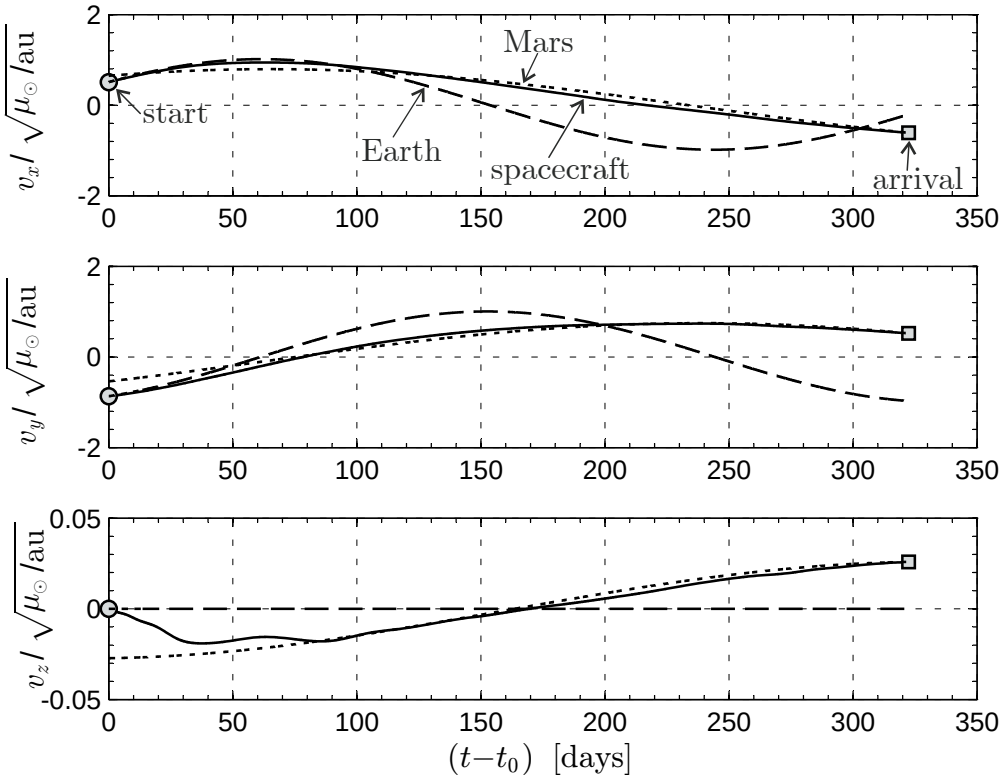

Figure 11. Dimensionless components (in the inertial frame) of the velocity vector as a function of time, for an Earth-Mars optimal transfer with $a_c = 1$ mm/s^2 and a starting date on 21 April 2016.

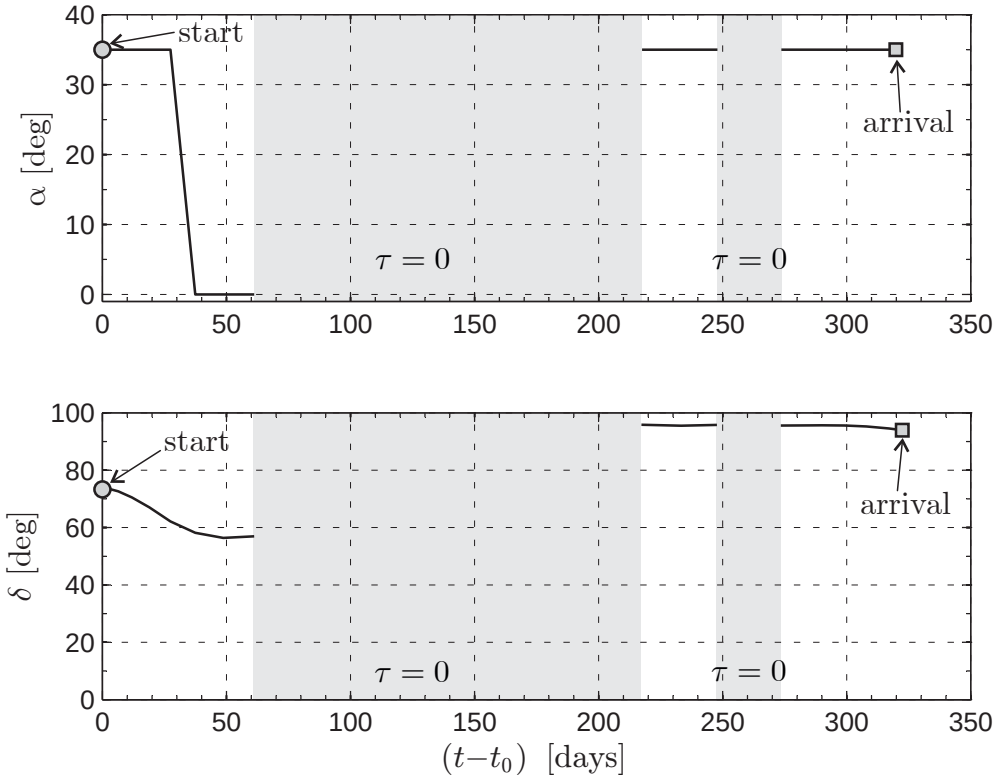

Figure 12. Thrust angles and switching parameter as a function of time, for an Earth-Mars optimal transfer with $a_c = 1$ mm/s^2 and a starting date on 21 April 2016.